Magnetocrystalline anisotropy in $L1_0$ FePt and exchange coupling in FePt/Fe_3Pt nanocomposites

2005 J. Phys.: Condens. Matter 17 4157

(http://iopscience.iop.org/0953-8984/17/26/014)

INSTITUTE OF PHYSICS PUBLISHING JOURNAL OF PHYSICS: CONDENSED MATTER

J. Phys.: Condens. Matter **17** (2005) 4157–4170 doi:10.1088/0953-8984/17/26/014

Magnetocrystalline anisotropy in $L1_0$ FePt and exchange coupling in FePt/Fe_3Pt nanocomposites

Julia Lyubina[1], Ingo Opahle, Karl-Hartmut Müller, Oliver Gutfleisch, Manuel Richter, Manfred Wolf and Ludwig Schultz

IFW Dresden, PO Box 270116, D-01171 Dresden, Germany

E-mail: j.lyubina@ifw-dresden.de

Received 3 May 2005, in final form 5 June 2005
Published 17 June 2005
Online at stacks.iop.org/JPhysCM/17/4157

Abstract

The magnetic and structural properties of Fe–Pt nanocomposites and related idealized structures have been investigated by a combination of experimental and theoretical techniques. The dependence of magnetocrystalline anisotropy (MCA) of $L1_0$ FePt on the ratio of the tetragonal lattice parameters, c/a, has been calculated with a relativistic version of the full potential local orbital method, assuming complete chemical order and fixed unit-cell volume. It has been found that the well known tetragonal lattice distortion in this phase has a relatively small influence on the MCA (compared to the influence of chemical ordering) and even reduces the MCA. The calculated in-plane anisotropy is negligible. The structure, magnetic properties and magnetization reversal processes of $Fe_{100-x}Pt_x$ ($x = 40$, 45, and 50) powders produced by mechanical milling and subsequent annealing have been investigated. Structural studies reveal that upon annealing of the as-milled powders consisting of fine Fe/FePt(A1)/Pt lamellae, chemically highly ordered $L1_0$ FePt and, in the case of the Fe-rich compositions, $L1_2$ Fe_3Pt are formed. The nanometre scale multilayer structure preserved after annealing gives rise to large effects of exchange interactions between the crystallites of the phases. With decreasing Pt concentration x, the remanence enhancement increases, due to the increase of the Fe_3Pt fraction, whereas the coercivity and the switching fields for irreversible magnetization reversal are reduced.

1. Introduction

In recent years, much attention has been devoted to the enhancement of remanent magnetization (remanence) and to the so-called spring-magnet hysteresis behaviour of nanocomposite

[1] Address for correspondence: Department of Magnetism and Superconductivity, Leibniz Institute for Solid State and Materials Research Dresden, IFW Dresden, Helmholtzstraße 20, D-01069 Dresden, Germany.

magnets both caused by exchange coupling between grains of different magnetic phases [1–4]. Careful control of the microstructure on a scale of nanometres is required to produce these phenomena. An important issue in understanding the magnetic properties and magnetization reversal processes of nanocomposite exchange coupled materials is the knowledge and control of dimensions, relative amounts and distribution of ferromagnetic phases with small and large magnetocrystalline anisotropy (MCA), in the following called soft and hard magnetic phases, respectively.

Due to its exceptional combination of excellent intrinsic magnetic properties, high ductility and good corrosion resistance, the tetragonal $L1_0$ FePt phase attracted much interest from both fundamental and application points of view [5–12]. The main intrinsic magnetic properties of this itinerant-electron ferromagnet are reported to be $T_c = 750$ K (Curie temperature), $J_s = 1.43$ T (spontaneous magnetization at room temperature) and $K_1 = 6.6$ MJ m^{-3} (first anisotropy constant at room temperature) [5, 6]. Hence the MCA of $L1_0$ FePt is larger than that of the rare-earth transition-metal compounds used in modern permanent magnets, $Nd_2Fe_{14}B$(4.9 MJ m^{-3}) and Sm_2Co_{17} (3.3 MJ m^{-3}). The reason for the strong MCA in $L1_0$ FePt is the large spin–orbit coupling in Pt and the 5d(Pt)–3d(Fe) hybridization, both together transforming the effect of the tetragonal lattice on the orbital electron wave functions into a strong dependence of the free energy on the direction of J_s mainly consisting of contributions from 3d(Fe) spins [13–15]. According to the equilibrium Fe–Pt phase diagram [16], $L1_0$ FePt forms from the disordered fcc phase A1 FePt by ordering the Fe and Pt atoms into a superstructure consisting of staggered Fe and Pt layers. If this chemical ordering were to take place without any lattice distortion the ratio of the lattice parameters in the tetragonal unit cell would be $c/a = 1.414$. In reality, however, c/a of $L1_0$ FePt is 1.363 [8]. The MCA will be influenced by both the chemical ordering and this lattice distortion. However, because these phenomena are strongly correlated with each other it would be difficult to experimentally separate their respective influences on the MCA. In the literature, this topic has been discussed controversially. Whereas in [9, 12] the lattice distortion has been considered as the main reason for the large MCA, in [14] it has been concluded from results of electronic structure calculations that the lattice distortion has a much smaller effect on the MCA than the effect of chemical ordering. Assuming the first scenario, even small deviations of the c/a-ratio in the nanocrystalline compound from its bulk value would have a strong influence on the MCA, disregarding the chemical ordering. In the second scenario, such effects would have only a moderate influence on the MCA. The second scenario will be confirmed by calculations done in this study.

In the equilibrium Fe–Pt phase diagram [16], at room temperature, besides $L1_0$ FePt, the phases $FePt_3$ and Fe_3Pt, both of $L1_2$-type structure, are present. The latter phase is ferromagnetic with a reported room-temperature value of its spontaneous magnetization as high as $J_s[Fe_3Pt] = 1.8$ T [17]. It should be noted, however, that the published values of $J_s[Fe_3Pt]$ scatter considerably. The Curie temperature of $L1_2$ Fe_3Pt is $T_c = 430$ K [18]. The combination of hard magnetic $L1_0$ FePt and soft magnetic Fe_3Pt yields a significant remanence enhancement in Fe_3Pt/FePt nanocomposites prepared by chemical synthesis [10]. Very high remanence values obtained in rapidly annealed thin-film Fe/Pt multilayers have also been reported [19], although the resulting nanocomposite film no longer exhibited the original multilayer structure. On the other hand, it has been confirmed in [17] that spring-magnet behaviour does not occur if the crystallite size in a $L1_0$FePt/$L1_2$ Fe_3Pt two-phase system is too large. Remanence enhancement has also been found in annealed bulk $Fe_{59.75}Pt_{39.5}Nb_{0.75}$ [11]. However, no typical spring-magnet behaviour was observed in these alloys, which was mainly attributed to an insufficient degree of order in the $L1_0$ phase. This confirms that despite the crystallographic simplicity of the $L1_0$ phase, its formation and the accomplishment of complete

chemical long-range order require sophisticated preparation procedures, which have not yet been investigated in full detail. In [20, 21] it has been demonstrated that a nanoscale multilayer-like structure can be obtained by mechanical milling at 77 K followed by heat treatment at moderate temperatures. The latter results in the formation of chemically highly ordered $L1_0$ FePt and, in the case of Fe-rich overall compositions, $L1_2$ Fe_3Pt phases. However, only a weakly pronounced exchange-spring behaviour was observed in the Fe-rich powders, which has been attributed to a specific layer distribution of the phases. It was suggested [21] that for an effective exchange coupling a finer lamellar structure of $L1_0$ FePt and Fe_3Pt would be needed.

In the present work, we investigate the effect of such structural features on the magnetic properties of nanocomposite FePt/Fe_3Pt powders. Also we compare results on the MCA of $L1_0$ FePt, experimentally determined for $Fe_{50}Pt_{50}$ powder, with those obtained by electronic structure calculations.

2. Theoretical and experimental methods

The dependence of the MCA on the c/a-ratio of $L1_0$ FePt was obtained from total energy differences calculated with the relativistic version [22] of the full potential local orbital method [23] (RFPLO). Chemical order was kept complete, independent of c/a. The volume of the unit cell was kept fixed to the experimental value. The Perdew–Wang [24] parameterization of the exchange–correlation (XC) potential in the local spin-density approximation (LSDA) was used. The basis set used in the calculations consisted of Fe 3spd and 4sp and Pt 5spd and 6sp states. For the **k**-space integrations, 32 768 points in the full Brillouin zone were used. The convergence of the MCA (ΔMCA $< 5\%$) with respect to the basis set and to the numerical parameters was carefully checked at the experimental value of the c/a-ratio.

$Fe_{100-x}Pt_x$ powders with overall compositions of $x = 40$, 45, and 50 were prepared by mechanical ball milling for 4 h at liquid nitrogen temperature followed by annealing at 450 °C as described previously [20]. The structure of the powders was investigated by x-ray diffraction (Philips X'Pert diffractometer equipped with a diffracted beam monochromator) using Co Kα radiation. Rietveld refinement (X'Pert Plus software) was used to determine the phase composition, the lattice parameters and the order parameter. A modified Williamson–Hall analysis, the so-called 'average size–strain' method [25], was applied to separate the contributions to the overall line breadth from the crystallite size $\langle D \rangle$ and lattice strain $\langle e \rangle$. The line profile parameters were extracted from the Rietveld refinement and corrected for instrumental broadening. As a standard reference material, a LaB_6 powder specimen was used. The powder microstructure was investigated by means of field emission gun scanning electron microscopy (SEM) by using a FEGSEM LEO 1530 device equipped with energy dispersive x-ray (EDX) analysis. The magnetic properties were measured using a SQUID (Quantum Design MPMS-5S) and a VSM with a maximum applied field of 6 T. To determine the MCA, magnetization curves were measured at 5 and 300 K in an extraction magnetometer with fields up to 16 T.

3. Results and discussion

3.1. Magnetic anisotropy in $L1_0$ FePt

Figure 1 shows the computed difference ΔE between the electronic energy per formula unit (fu) of zero-temperature states with magnetization J_s parallel to the c-axis and parallel to the a-axis, $\Delta E = E(J_s \parallel c) - E(J_s \parallel a)$, for completely ordered $L1_0$ FePt. The calculation was carried

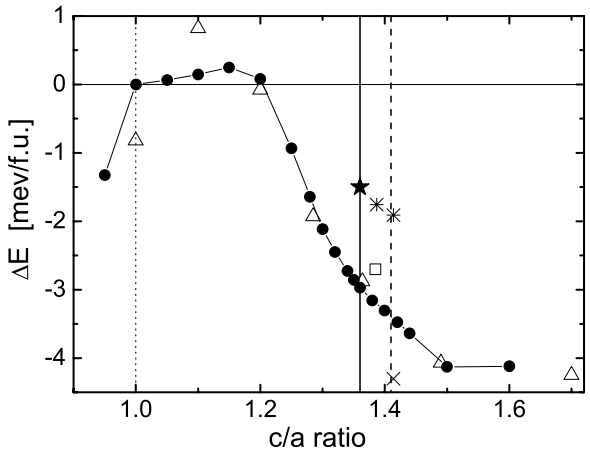

Figure 1. Calculated values of MCA energy ΔE of $L1_0$ FePt (closed symbols) as a function of c/a-ratio. The vertical full line marks the experimental value of c/a, whereas the dashed line represents the fully ordered but non-distorted material and the dotted line marks the cubic CsCl-type structure. For comparison calculated values from the literature ($\times$ [14], $*$ [15], $\triangle$ [29] and $\square$ [26, 30]) and the experimental value ($\bigstar$) determined at 5 K for $Fe_{50}Pt_{50}$ powder (annealed at 450 °C/336 h) are also given.

out for different c/a at fixed unit cell volume of 27.5 Å^3, corresponding to the experimentally determined lattice parameters $c = 3.71$ Å and $a = 2.72$ Å [8]. Note that the experimental c/a-ratio is about 1.36, whereas several recent calculations were carried out with the different value 1.39 (e.g. [26, 27]). If a tP4 (Pearson symbol) pseudocell with the lattice parameters $c' = c$ and $a' = \sqrt{2}a$ were to be used instead of the correct tP2 unit cell the experimental c'/a'-ratio would be 0.96. It should be noted that $L1_0$ structures without the above-mentioned lattice distortions, i.e. for identical in-plane and out-of-plane atomic distances, $c'/a' = 1$ (as for example in FeNi [26]), are nevertheless clearly tetragonal with $c/a = \sqrt{2}$.

Obviously, the calculation correctly yields easy-axis magnetic anisotropy. The calculated value of ΔE at the experimental c/a-ratio is about -2.9 meV fu^{-1}, whereas the in-plane anisotropy ($E_{110} - E_{100}$) is found to be about 100 times smaller. The LSDA lattice parameters $a = 2.68$ Å and $c/a = 1.38$ obtained from the minimization of the total energy $E(a, c/a)$ deviate by less than 2% from the experimental values. Compared to the measured MCA data at low temperatures (see section 3.2) the calculated ΔE is about a factor of two larger. This is in agreement with earlier LSDA calculations and in contrast to the results for $L1_0$ CoPt, where the LSDA calculations reproduce the measured anisotropy energy within the scatter of the experimental results. The discrepancy between theory and experiment for $L1_0$ FePt could be due to a failure of the LSDA to accurately reproduce such small energy differences, but there may also be another source for the deviation. The measured anisotropy energy depends quite delicately on the quality of the sample, described for example by the degree of chemical order S,

$$S = r_{Pt} + r_{Fe} - 1 \tag{1}$$

with r_{Pt} and r_{Fe} as the fractions of sites correctly occupied by the two types of atoms [28]. Measurements on fully ordered bulk samples have probably not yet been carried out, so that values for fully ordered crystals have to be extrapolated, which however gives rise to uncertainties. It can be seen from figure 1 that a lattice distortion of about 4% has only a moderate effect (of about 15%) on the whole MCA. The main effect on the MCA results from

the symmetry change from cubic to tetragonal caused by chemical ordering. In completely disordered A1 FePt the MCA is orders of magnitude smaller [15], because for cubic systems the strength of spin–orbit interaction enters in fourth order in terms of perturbation theory whereas in tetragonal systems there is a second-order contribution. As can be seen in figure 1, the lattice distortion (from $c/a = 1.41$ to 1.36) even reduces the MCA, which is not surprising as the distortion obviously reduces the degree of tetragonality. A further reduction of c/a down to 1 results in the cubic $B2$-type (i.e. CsCl-type) structure with weak (fourth-order) MCA. For $c/a = 1$, $J_s \parallel c$ and $J_s \parallel a$ are equivalent by symmetry and ΔE must exactly vanish, which is accurately reproduced by the calculations (see figure 1). Nevertheless, there is a small anisotropy energy $E_{001} - E_{111} \approx -0.07$ meV. For c/a around 1.1, $(E_{001} - E_{100})$ even changes sign. Figure 1 also shows a comparison with the results of other recent MCA calculations [14, 15, 26, 29, 30]. As can be seen, there is a large scattering of values calculated with different band structure codes (or modifications of the same code [14, 15]). A small fraction of these deviations (about 0.1 meV, according to our test calculations) may be attributed to different parameterizations of the DFT functional in use. The remaining differences must be due to numerical inaccuracies (basis set, potential construction, etc). This is in strong contrast to sometimes claimed accuracies of better than 1 μeV [14]. Nevertheless, a couple of results obtained using high-accuracy codes yield values of -2.8 ± 0.3 meV. This reasonably small scatter originates from the use of slightly different lattice geometries, and different parameterizations of the LSDA exchange and correlation potential, as well as different electronic structure codes. In real systems the order parameter, equation (1), and the lattice distortion increase simultaneously upon chemical ordering. Therefore a seeming increase of MCA with increasing lattice distortion is observed if the order parameter S is not fixed during the experiment [15, 31]. It would be difficult to experimentally separate the effect of the lattice distortion on MCA from the effect of chemical ordering. If a pure uniaxial distortion (not accompanied by chemical ordering) were to be applied to completely disordered A1 FePt, a change of symmetry from cubic to tetragonal would be induced, resulting in an A6-type structure (Pearson symbol tI2). *Ab initio* calculations have shown that, as expected, in such a case the tetragonal distortion would strongly increase the MCA [14].

3.2. Nanocomposite materials based on $L1_0$ FePt

A fine lamellar microstructure with a layer thickness in the range 90–10 nm is obtained as a result of milling. Figure 2 shows an SEM image of the as-milled $Fe_{60}Pt_{40}$ powder, where three types of compositional contrast can be distinguished: Pt, Fe and FePt. Quantitative phase analysis of the as-milled $Fe_{100-x}Pt_x$ ($x = 40$, 45, and 50) powders using Rietveld refinement confirms that the powder is a mixture of α-Fe, Pt and disordered A1 FePt (55–65 vol%) phases. The appearance of the latter phase is a result of alloying at this milling stage.

As shown in [21, 32], heat treatment of the as-milled Fe–Pt powders with the lamellar microstructure induces so-called combined solid-state reactions. Such reactions take place in solids in which thermodynamical equilibrium is approached by more than one elementary reaction [33]. This leads simultaneously to a decrease of defect density and to nucleation and growth of new phases concurrent with the ordering process. Figure 3 shows phase compositions of the heat-treated $Fe_{100-x}Pt_x$ ($x = 40$, 45, and 50) powders, as determined by Rietveld refinement. The dominant phase identified in all the powders is ordered $L1_0$ FePt. Its fraction reaches a maximum of about 97.2(6) vol% in the $Fe_{50}Pt_{50}$ powder (450 °C/336 h), the rest being disordered FePt (A1) phase. As an example, figure 4 shows an x-ray diffraction pattern of this sample. In the Fe-rich powders, along with the $L1_0$ FePt and A1 FePt phases, the Fe_3Pt phase was detected. Its amount increases from about 6 vol% for $Fe_{55}Pt_{45}$ to 30 vol% for $Fe_{60}Pt_{40}$.

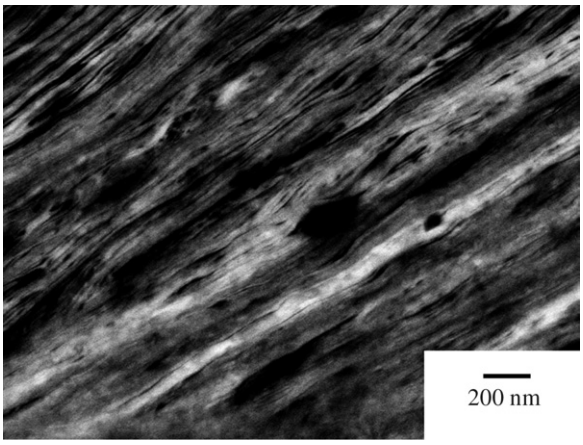

Figure 2. High-resolution SEM image (backscattered electron mode) of a particle of the $Fe_{60}Pt_{40}$ powder milled at 77 K for 4 h. Three types of compositional contrast are observed: dark contrast—Fe; grey—$Fe_{50}Pt_{50}$, bright—Pt.

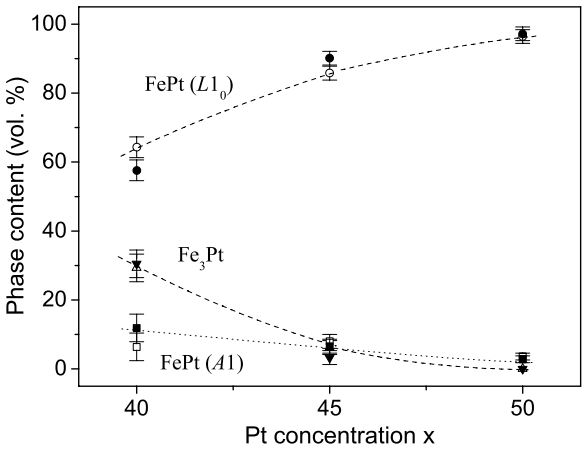

Figure 3. The dependence of the phase composition of the $Fe_{100-x}Pt_x$ powders annealed at 450 °C for 48 h (open symbols) and for 336 h (solid symbols) on Pt concentration x (the lines are guides to the eye).

Because of the relatively small Fe_3Pt volume fraction and very similar lattice parameters of the phases, it is difficult to unambiguously distinguish whether the observed $Fe_{75}Pt_{25}$ phase has ordered $L1_2$ or disordered A1 structure. Nevertheless, Rietveld refinement of the x-ray diffraction spectra of the Fe-rich $Fe_{100-x}Pt_x$ powders allows the identification of two cubic phases with different lattice parameters. The first one, presumably $L1_2$ Fe_3Pt, has almost the same lattice parameters in both $Fe_{60}Pt_{40}$ and $Fe_{55}Pt_{45}$ powders: $a = 3.775(1)$ Å and $a = 3.774(2)$ Å, respectively. At the same time, the lattice constant of the disordered FePt (A1) phase changes with Pt concentration: it increases from $a = 3.801(1)$ Å for $Fe_{60}Pt_{40}$ to $a = 3.824(2)$ Å for $Fe_{50}Pt_{50}$. This means that the atomic composition of the A1 FePt phase is slightly modified with x. The lattice parameters of the $L1_0$ phase (tP4 unit cell) change with Pt concentration as well: a' increases from 3.8406(1) to 3.8605(2) Å, and c' is reduced from 3.7202(9) to 3.7139(3) Å if x changes from 40 to 50.

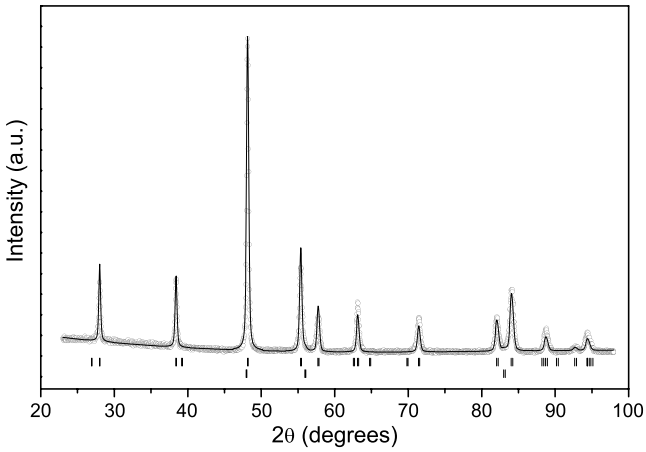

Figure 4. Observed (○) and calculated (full line) x-ray diffraction profiles of the $Fe_{50}Pt_{50}$ powder annealed at 450 °C/336 h. The vertical bars represent the Bragg reflection positions of the observed phases (from top to bottom: $L1_0$ and A1).

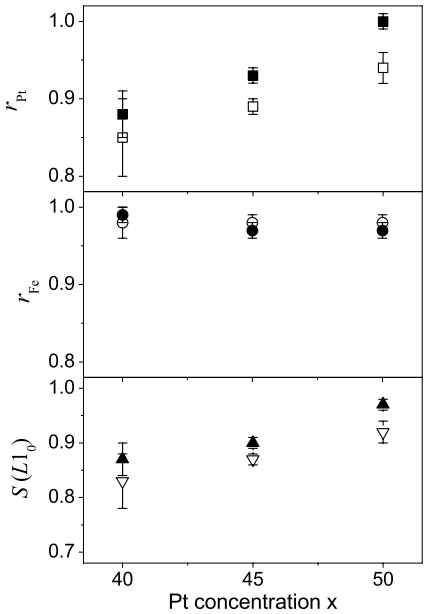

Figure 5. The fractions r_{Pt} and r_{Fe} of Pt and Fe sites, respectively, occupied by a correct atom and the order parameter S of the $L1_0$ FePt phase in the $Fe_{100-x}Pt_x$ powders annealed for 48 h (open symbols) and for 336 h (solid symbols) at 450 °C.

Rietveld analysis was also employed for the investigation of site occupations in the $L1_0$ FePt phase and its evolution with Pt concentration in the $Fe_{100-x}Pt_x$ powders. The fractions of the Pt(Fe) sites occupied by the right atom $r_{Pt(Fe)}$, extracted from the Rietveld refinement, were used for the determination of the long-range order parameter S of $L1_0$ FePt, as defined in equation (1). The fractions of correctly occupied sites and order parameter of the $L1_0$ FePt phase are shown in figure 5. The site occupation fractions are high for all the powders. The r_{Fe}

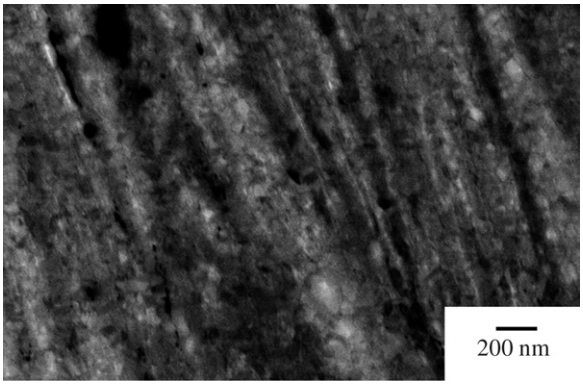

Figure 6. High-resolution SEM image (backscattered electron mode) of the $Fe_{55}Pt_{45}$ powder (annealed at 450 °C for 48 h). Bright contrast areas have a stoichiometry of $Fe_{50}Pt_{50}$, dark contrast areas are $Fe_{75}Pt_{25}$.

Table 1. Values of the spontaneous magnetization J_s, the anisotropy field H_a and the first anisotropy constant K_1 determined from magnetization curves using the law of approach to saturation at 5 and 300 K for $Fe_{50}Pt_{50}$ powder (annealed at 450 °C/336 h).

T (K)	J_s (T)	$\mu_0 H_a$ (T)	K_1 (MJ m^{-3})
5	1.5(1)	14.8(5)	8.7(9)
300	1.39(5)	13.0(5)	7.0(7)

fraction is about 0.98 and is relatively independent of x. However, the fraction of the correctly occupied Pt sites in the $L1_0$ structure increases from $r_{Pt} = 0.85(5)$ for $Fe_{60}Pt_{40}$ to 0.94(2) for $Fe_{50}Pt_{50}$ in the powders annealed at 450 °C/48 h. Consequently, the order parameter of the $L1_0$ phase increases from 0.83 ($x = 40$) to 0.92 ($x = 50$).

While no considerable differences in the lattice parameters and volume fractions (see figure 3) of the phases are observed with increasing the annealing time to 336 h, the site occupation r_{Pt} in the $L1_0$ FePt phase and, accordingly, the $L1_0$ order parameter slightly increase (solid symbols in figure 5). The order parameter S reaches a maximum value of 0.97(1) for the $Fe_{50}Pt_{50}$ powder.

In a simple phenomenological description [5] the MCA is characterized by the anisotropy constant

$$K_1 = \frac{H_a J_s}{2}, \tag{2}$$

where H_a is the anisotropy field. The values of H_a and J_s determined from the fit of magnetization curves using the law of approach to saturation are listed in table 1. For $Fe_{50}Pt_{50}$ annealed at 450 °C for 336 h, K_1 of $L1_0$ FePt was found to be 7.0 ± 0.7 MJ m^{-3} and 8.7 ± 0.9 MJ m^{-3} at 300 and 5 K, respectively. This corresponds to ΔE equal to -1.2 ± 0.1 and -1.5 ± 0.1 meV fu^{-1}, respectively. These values are in good agreement with reported experimental values [6, 34] and a factor of two lower than those obtained by LSDA calculations (figure 1).

The phases in the annealed $Fe_{100-x}Pt_x$ powders are distributed in a form of fine lamellae, i.e. the nanometre scale multilayer structure is preserved even after annealing. As an example, figure 6 shows a high-resolution SEM image of the $Fe_{55}Pt_{45}$ powder (450 °C/48 h), where two types of contrast are observed. These areas have the stoichiometry of $Fe_{75}Pt_{25}$ and $Fe_{50}Pt_{50}$,

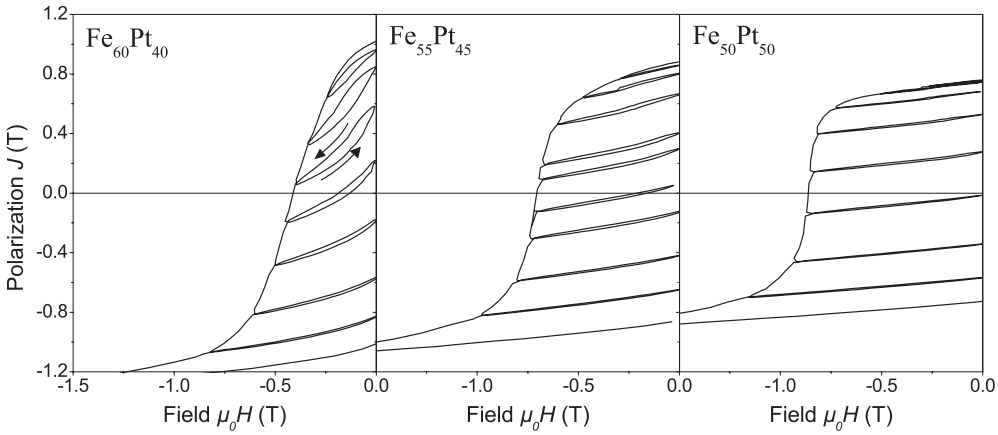

Figure 7. Demagnetization curves and recoil loops of $Fe_{100-x}Pt_x$ ($x = 40$, 45, and 50) powders (annealed at 450 °C for 48 h), measured at 300 K.

as identified by EDX analysis. The high-resolution SEM analysis agrees with the phase analysis of the x-ray diffraction patterns by the Rietveld method. The average grain size $\langle D \rangle$ of the $L1_0$ FePt phase determined from the x-ray data is about 30–35 nm. In the Fe-rich $Fe_{100-x}Pt_x$ powders, the crystallite size of the Fe_3Pt phase is slightly lower, namely about 20 nm. Such a microstructure is an excellent prerequisite for intense exchange interactions between crystallites of hard magnetic $L1_0$ FePt and soft magnetic $L1_2$ Fe_3Pt and A1 FePt phases in the $Fe_{100-x}Pt_x$ powders.

Figure 7 shows demagnetization curves and recoil loops of the $Fe_{100-x}Pt_x$ powders annealed at 450 °C for 48 h. Although there are several magnetic phases present in the powders, their demagnetization curves do not reveal dips or steps, i.e. the powders show a *single-phase magnetic* behaviour. Moreover, the recoil loops of the Fe-rich powders are rather steep and, at the same time, they are fairly reversible, i.e. they indicate exchange-spring-magnet behaviour [3]. Differently from ideal exchange-spring-magnet behaviour, the recoil loops of the $Fe_{60}Pt_{40}$ powder are slightly open, indicative of a non-vanishing magnetic anisotropy of the soft-magnetic phases (Fe_3Pt and A1 FePt) exchange coupled to the hard magnetic $L1_0$ FePt. The origin of this anisotropy is not yet well understood. Possible contributions may arise from shape anisotropy as well as surface anisotropy of the fine soft magnetic lamellae.

For an assembly of non-interacting ferromagnetic randomly oriented particles, the remanence-to-saturation ratio J_r/J_s is equal to 0.5 for uniaxial magnetocrystalline anisotropy and $J_r/J_s = 0.832$ in the case of cubic symmetry (for anisotropy constant $K_1 > 0$). Accordingly, the remanent polarization J_r in the $Fe_{100-x}Pt_x$ powders if consisting of non-interacting particles of $L1_0$ FePt, $L1_2$ Fe_3Pt and A1 FePt, can be calculated using

$$J_r = 0.5 J_s^{L1_0} f_{L1_0} + 0.832 (J_s^{Fe_3Pt} f_{Fe_3Pt} + J_s^{A1} f_{A1}), \tag{3}$$

where $J_s^{L1_0} = 1.43$ T, $J_s^{Fe_3Pt} \approx 1.8$ T and $J_s^{A1} \approx 1.5$ T [35] are the room-temperature values of spontaneous polarization of the three phases and f_{L1_0}, f_{Fe_3Pt} and f_{A1} are volume fractions of the phases. The remanence values calculated in this manner are considerably lower than the experimental ones (see figure 8), thus pointing towards the presence of exchange interactions in the system. The difference between the estimated and experimental J_r values increases with decreasing Pt content, indicating an increase of remanence enhancement due to the increase of the Fe_3Pt fraction.

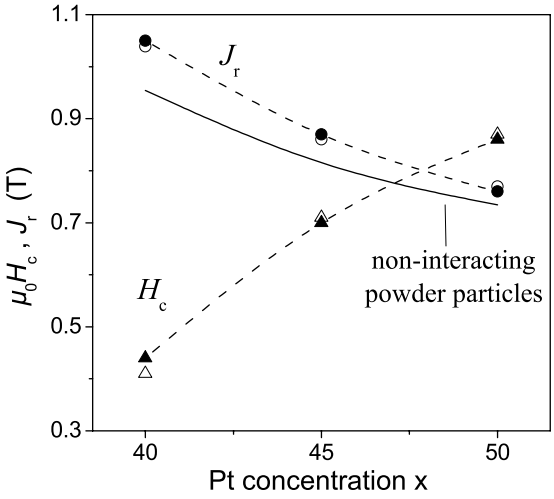

Figure 8. The dependence of the room-temperature remanence J_r and coercivity H_c of the $Fe_{100-x}Pt_x$ powders annealed at 450 °C for 48 h (open symbols) and for 336 h (solid symbols) on Pt concentration x and J_r values calculated using equation (3).

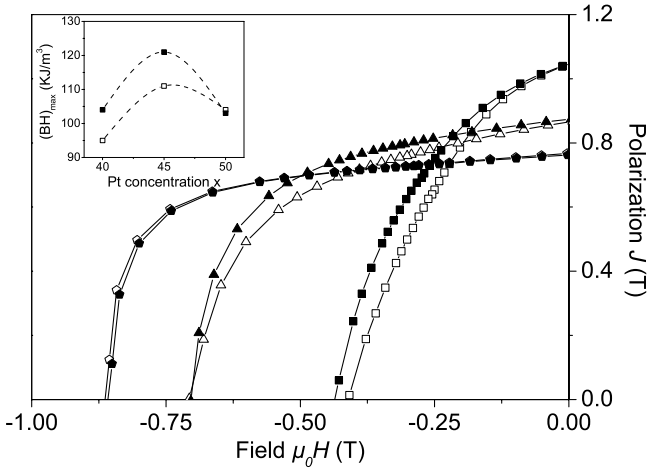

Figure 9. The dependence of the demagnetization curves (at 300 K) of the $Fe_{100-x}Pt_x$ powders annealed at 450 °C for 48 h (open symbols) and for 336 h (solid symbols) on Pt concentration x. Inset: the dependence of the energy density $(BH)_{max}$ on x.

With increasing Pt concentration x, the coercivity (defined as $J(H) = 0$ at $H = -H_c$) of the $Fe_{100-x}Pt_x$ powders annealed at 450 °C for 48 h increases from 0.41 to 0.87 T, whereas the remanence J_r decreases from 1.04 to 0.77 T for x increasing from 40 to 50 (figure 8). The maximum energy density $(BH)_{max}$ is highest for $Fe_{55}Pt_{45}$ (see the inset of figure 9). An increase of annealing time to 336 h influences the values of remanence and coercivity only slightly (it has to be noted that an extension of annealing time to 336 h does not lead to any noticeable grain growth). Nevertheless, the maximum energy density of the Fe-rich $Fe_{100-x}Pt_x$ powders increases markedly (figure 9). This may be due to the increase of S in the $L1_0$ FePt phase, resulting in an increase of the MCA [15, 31]. The increase of $L1_0$ anisotropy together with the exchange coupling between the soft and the hard phases will result in an improved squareness

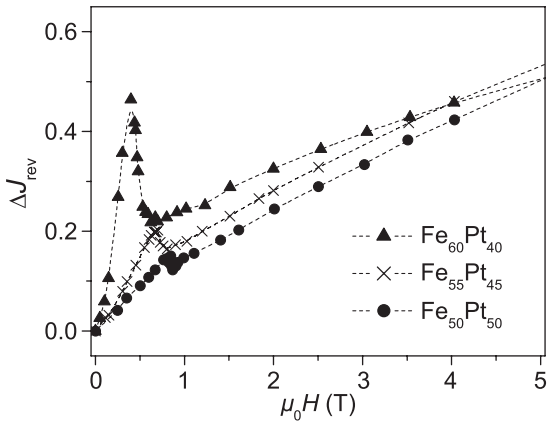

Figure 10. Variation (at 300 K) of the reversible (ΔJ_{rev}) portion of the change in polarization, defined by equation (4), as a function of the maximum applied reverse magnetic field H in the $Fe_{100-x}Pt_x$ powders annealed at 450 °C for 336 h.

of the demagnetization curves and, as a consequence, in the higher energy density $(BH)_{max}$. In $Fe_{50}Pt_{50}$ powders, where the fractions of the soft magnetic A1 FePt phase are negligible, the shape of the hysteresis loop remains unchanged, i.e. the increase of S does not influence the effect of intergrain coupling in this essentially single-phase hard magnetic material.

One of the characteristics of exchange-spring-magnet materials is the (nearly) reversible rotation of the magnetically soft component of magnetization at fields below the switching field of the hard magnetic phase. In order to examine how the magnetization reversal processes in the $Fe_{100-x}Pt_x$ powders are affected by the Pt concentration x or, in other words, by the soft magnetic phase fraction, the dc demagnetization curves were investigated in terms of reversible and irreversible portions of the total polarization change as functions of an applied reverse (i.e. negative) field H [3]. The reversible portion of the change of polarization is given by

$$\Delta J_{rev}(H) = [J_d(H) - J(H)]/J_r, \tag{4}$$

while the irreversible portion of polarization change,

$$\Delta J_{irr}(H) = [J_r - J_d(H)]/2J_r, \tag{5}$$

is the change in remanent polarization after the reverse field has been removed. Here $J(H)$ is the polarization obtained after saturation and subsequent application of the reverse field H and $J_d(H)$ is the remanence obtained after removal of H. The reversible portion of the polarization change was found to increase with increasing soft magnetic phase content (figure 10). The switching field distribution (SFD) obtained by using the irreversible susceptibility $\chi_{irr} = d(\Delta J_{irr})/dH$ is shown in figure 11. The single peak in χ_{irr} at the nucleation field H_n suggests a one-stage magnetization reversal process and manifests the single-phase magnetic behaviour, mentioned above. Obviously, the reversal of magnetization takes place as a cooperative process due to the intergrain exchange coupling. A shift in the mean value H_n to higher values occurs with increasing x, i.e. with decreasing soft magnetic phase fraction. Moreover, the SFDs are narrowed with increasing x, indicative of a more uniform switching as the soft magnetic phase fraction is reduced (see table 2). These observations show that the soft phases not only increase the value of remanence but, due to the intergrain exchange coupling, they also modify the switching behaviour of the hard magnetic grains.

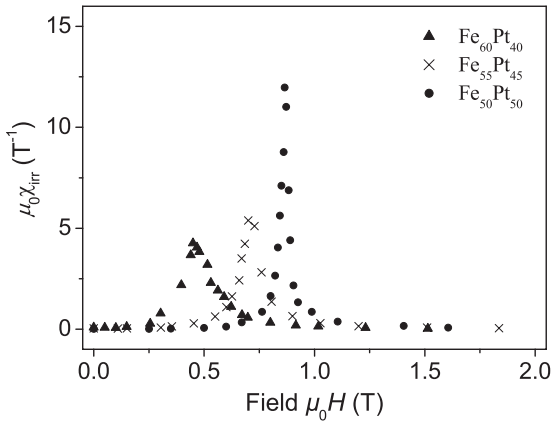

Figure 11. Irreversible susceptibility $\chi_{irr} = d(\Delta J_{irr})/dH$, measured at 300 K, of the $Fe_{100-x}Pt_x$ powders annealed at 450 °C for 336 h as a function of the field for different concentrations x, representing the switching field distribution (SFD).

Table 2. Room-temperature switching field distribution (SFD) parameters of the $Fe_{100-x}Pt_x$ powders annealed at 450 °C for 336 h. HW is the full-width-at-half-height parameter of the SFD. The SFD has its maximum at the nucleation field H_n.

	$\mu_0 H_n$ (T)	HW (T)
$Fe_{60}Pt_{40}$	0.468(3)	0.17(1)
$Fe_{55}Pt_{45}$	0.712(1)	0.099(3)
$Fe_{50}Pt_{50}$	0.866(1)	0.042(2)

Due to their relationship to purely irreversible magnetization changes, remanence curves may be used to provide insight into the nature of magnetic interactions [36, 37]. The analysis of the interparticle interactions in the $Fe_{100-x}Pt_x$ powders was carried out using ΔJ curves [38], given by

$$\Delta J(H) = \frac{J_d(H) - [J_r - 2J_r(H)]}{J_r}, \tag{6}$$

where $J_r(H)$ is the isothermal (non-saturated) remanent polarization measured after a field H had been applied to the (thermally or ac-field-) demagnetized sample and then the field has been removed. Consequently it follows $J_r(\infty) = J_r$ as the (saturated) remanence of the material. Non-vanishing $\Delta J(H)$ values are considered to be indicative for the presence of magnetic interactions. Positive $\Delta J(H)$ are interpreted as being due to exchange (magnetizing type) interactions and negative $\Delta J(H)$ to magnetostatic (demagnetizing type) interactions [38, 39]. Predominantly positive values of $\Delta J(H)$ are observed in the $Fe_{100-x}Pt_x$ powders (figure 12), pointing to the presence of intergranular exchange interactions. It should be noted, however, that this conclusion is only tentative. For certain types of short-range order in an assembly of magnetostatically interacting particles $\Delta J(H)$ can be positive as well. Furthermore, strictly speaking, the Wohlfarth relation $\Delta J(H) \neq 0$ can only be used to analyse interactions between magnetic particles if these are single-domain and of uniaxial type of magnetic anisotropy. Hence non-homogeneous magnetization modes such as magnetic domain structures and easy-plane as well as cubic magnetic anisotropy have to be excluded. On the other hand, $\Delta J(H) = 0$ does not necessarily imply the absence of magnetic interactions between the particles. Thus in an ideal exchange-spring-magnet the switching behaviour of the soft magnetic crystallites is

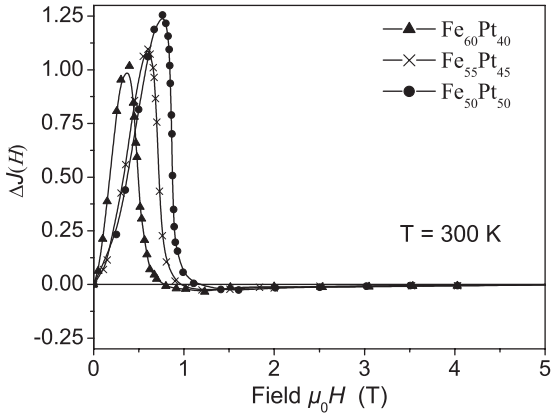

Figure 12. $\Delta J(H)$ plots for the $Fe_{100-x}Pt_x$ powders annealed at 450 °C for 336 h for various values of x.

strongly modified by the exchange interaction with hard magnetic grains. Nevertheless, most of the soft grains will not contribute to finite values of $\Delta J(H)$.

4. Conclusions

The magnetocrystalline anisotropy (MCA) of $L1_0$ FePt can be well understood and calculated using the full potential local orbital method for electronic structure calculations. The MCA is mainly caused by the chemical ordering of Fe and Pt atoms into staggered layers, whereas the lattice distortion accompanying the chemical order has only a minor influence on the MCA. The experimentally deduced MCA for nanocrystalline $Fe_{50}Pt_{50}$, mainly consisting of chemically well but not completely ordered $L1_0$ FePt, is a factor of two lower compared to the calculated value of -2.9 meV fu^{-1}. The electronic structure calculations show that the in-plane MCA in the tetragonal basal plane is about two orders of magnitude smaller.

In the case of Fe-rich $Fe_{100-x}Pt_x$ powders, exchange-spring nanocomposites composed of highly ordered hard magnetic $L1_0$ FePt and soft magnetic phases ($L1_2$ Fe_3Pt and A1 FePt) were obtained. The switching behaviour of both phases is strongly modified by exchange interactions between the grains. With decreasing Pt concentration x in $Fe_{100-x}Pt_x$, an increase of the remanence enhancement due to the increase of the Fe_3Pt fraction is observed, whereas the coercivity and the switching fields for irreversible magnetization reversal processes are reduced. The switching field distribution functions are broadened with decreasing x. This is attributed to an increasing influence of the soft magnetic Fe_3Pt phase on the switching process in $L1_0$ FePt. The analysis of intergrain interactions points to a dominance of exchange interactions in the $Fe_{100-x}Pt_x$ powders studied. Due to the opposite dependences of remanence and coercivity on the Pt content, the highest maximum energy density $(BH)_{max}$ is obtained for moderately off-stoichiometric powders, $x = 45$.

Acknowledgment

This work has been supported by the Deutsche Forschungsgemeinschaft (SFB 463, B6 and B11).

References

[1] Coehoorn R, de Mooij D B, Duchateau J P W B and Buschow K H J 1988 *J. Physique Coll.* **49** C8 669
[2] Eckert D, Handstein A, Müller K-H, Hesske R, Schneider J, Mattern N and Illgen L 1990 *Mater. Lett.* **9** 289

[3] Kneller E F and Hawig R 1991 *IEEE Trans. Magn.* **27** 3588
[4] Fullerton E F, Jiang J S and Bader S D 1999 *J. Magn. Magn. Mater.* **200** 392
[5] Skomski R and Coey J M D 1999 *Permanent Magnetism* (Bristol: Institute of Physics Publishing)
[6] Ivanov O A, Solina L V, Demshina V A and Magat L M 1973 *Fiz. Met. Metalloved.* **35** 92
[7] Sun S, Murray C B, Weller D, Folks L and Moser A 2000 *Science* **287** 1989
[8] Cebollada A, Farrow R F C and Toney M F 2002 *Magnetic Nanostructures* ed H S Nalwa (Stevenson Ranch, CA: American Scientific) p 93
[9] Weller D, Moser A, Folks L, Best M E, Lee W, Toney M F, Schwickert M, Thiele J-U and Doerner M F 2000 *IEEE Trans. Magn.* **36** 10
[10] Zeng H, Li J, Liu J P, Wang Z L and Sun S 2002 *Nature* **420** 395
[11] Xiao Q F, Brück E, Zhang Z D, de Boer F R and Buschow K H J 2004 *J. Alloys Compounds* **364** 315
[12] Rellinghaus B, Stappert S, Acet M and Wassermann E F 2003 *J. Magn. Magn. Mater.* **266** 142
[13] Daalderop G H O, Kelly P J and Schurmanns M F H 1991 *Phys. Rev.* B **44** 12054
[14] Ostanin S, Razee S S A, Staunton J B, Ginatempo B and Bruno E 2003 *J. Appl. Phys.* **93** 453
[15] Staunton J B, Ostanin S, Razee S S A, Gyorffy B, Szunyogh L, Ginatempo B and Bruno E 2004 *J. Phys.: Condens. Matter* **16** S5623
[16] Massalski T B (ed) 1990 *Binary Alloy Phase Diagrams* (Metals Park, OH: ASM International) p 1752
[17] Hai N H, Dempsey N M and Givord D 2003 *J. Magn. Magn. Mater.* **262** 353
[18] Kouvel J S 1967 *Intermetallic Compounds* ed J H Westbrook (New York: Wiley) p 529
[19] Liu J P, Luo C P, Liu Y and Sellmyer D J 1998 *Appl. Phys. Lett.* **72** 483
[20] Lyubina J, Gutfleisch O, Müller K-H, Schultz L and Dempsey N M 2004 *J. Appl. Phys.* **95** 7474
[21] Lyubina J, Gutfleisch O, Müller K-H and Schultz L 2005 *J. Magn. Magn. Mater.* **290/291** 547
[22] Eschrig H, Richter M and Opahle I 2004 *Relativistic Electronic Structure Theory—Part II: Applications* ed P Schwerdtfeger (Amsterdam: Elsevier) pp 723–76
[23] Koepernik K and Eschrig H 1999 *Phys. Rev.* B **59** 1743 (http://www.FPLO.de)
[24] Perdew J P and Wang Y 1992 *Phys. Rev.* B **45** 13244
[25] Langford J I 1992 *Proc. Int. Conf.: Accuracy in Powder Diffraction II* ed E Prince and J K Stalick (Washington, DC: US Government Printing Office) p 110 (NIST Special Publication No. 846)
[26] Ravindran P, Kjekshus A, Fjellvåg H, James P, Nordström L, Johannson B and Eriksson O 2001 *Phys. Rev.* B **63** 144409
[27] Galanakis I, Alouani M and Dreyssé H 2000 *Phys. Rev.* B **62** 6475
[28] Warren B E 1990 *X-ray Diffraction* (New York: Dover)
[29] Sakuma A 1994 *J. Phys. Soc. Japan* **63** 3053
[30] Shick A B and Mryasov O N 2003 *Phys. Rev.* B **67** 172407
[31] Kanazawa H, Lauhoff G and Suzuki T 2000 *J. Appl. Phys.* **87** 6143
[32] Lyubina J, Gutfleisch O, Skomski R, Müller K-H and Schultz L 2005 *Scr. Mater.* **53** 469
[33] Hornbogen E 1979 *Metall. Trans.* A **10** 947
[34] Hai N H, Dempsey N M and Givord D 2003 *IEEE Trans. Magn.* **39** 2914
[35] Menshikov A, Tarnóczi T and Krén E 1975 *Phys. Status Solidi* a **28** K85
[36] Wohlfarth E P 1958 *J. Appl. Phys.* **29** 595
[37] Henkel O 1964 *Phys. Status Solidi* **7** 919
[38] Mayo P I, O'Grady K, Kelly P E, Cambridge J, Sanders I L, Yogi T and Chantrell R W 1991 *J. Appl. Phys.* **69** 4733
[39] Chen Z, Zhang Y and Hadjipanayis G C 2000 *J. Magn. Magn. Mater.* **219** 178